

The first outburst of the new magnetar candidate SGR 0501+4516

N. Rea^{1*}, G. L. Israel², R. Turolla^{3,4}, P. Esposito^{5,6}, S. Mereghetti⁵, D. Götz⁷,
S. Zane⁴, A. Tiengo⁵, K. Hurley⁸, M. Feroci⁹, M. Still⁴, V. Yershov⁴, C. Winkler¹⁰,
R. Perna¹¹, F. Bernardini², P. Ubertini⁸, L. Stella², S. Campana¹², M. van der Klis¹,
P. Woods¹³

¹ *Astronomical Institute “Anton Pannekoek”, University of Amsterdam, Kruislaan 403, 1098SJ, Amsterdam, The Netherlands*

² *INAF – Osservatorio Astronomico di Roma, via Frascati 33, 00040, Monte Porzio Catone (RM), Italy*

³ *Università di Padova, Dipartimento di Fisica, via Marzolo 8, I-35131 Padova, Italy*

⁴ *Mullard Space Science Laboratory, University College London, Holmbury St. Mary, Dorking, Surrey, RH5 6NT, UK*

⁵ *INAF – Istituto di Astrofisica Spaziale e Fisica Cosmica, via E. Bassini 15, I-20133, Milano, Italy*

⁶ *INFN – Istituto Nazionale di Fisica Nucleare, Sezione di Pavia, via A. Bassi 6, 27100 Pavia, Italy*

⁷ *CEA Saclay, DSM/Irfu/Service d’Astrophysique, Orme des Merisiers, Bât. 709, 91191 Gif sur Yvette, France*

⁸ *University of California, Space Sciences Laboratory, 7 Gauss Way, 94720-7450 Berkeley, USA*

⁹ *INAF – Istituto di Astrofisica Spaziale e Fisica Cosmica, via Fosso del Cavaliere 100, I-00133 Rome, Italy*

¹⁰ *Astrophysics Division, Research and Scientific Support Department, ESA-ESTEC, Keplerlaan 1, 2201 AZ Noordwijk, The Netherlands*

¹¹ *JILA, University of Colorado, Boulder, CO 80309-0440, USA*

¹² *INAF – Osservatorio Astronomico di Brera, Via Bianchi 46, I-23807 Merate (Lc), Italy*

¹³ *Dynetics, Inc., 1000 Explorer Boulevard, Huntsville, AL 35806, USA*

16 August 2018

ABSTRACT

We report here on the outburst onset and evolution of the new Soft Gamma Repeater SGR 0501+4516. We monitored the new SGR with *XMM-Newton* starting on 2008 August 23, one day after the source became burst-active, and continuing with 4 more observations in the following month, with the last one on 2008 September 30. Combining the data with the *Swift*-XRT and *Suzaku* data we modelled the outburst decay over a three months period, and we found that the source flux decreased exponentially with a timescale of $t_c = 23.8$ days. In the first *XMM-Newton* observation a large number of short X-ray bursts were observed, the rate of which decayed drastically in the following observations. We found large changes in the spectral and timing behavior of the source during the first month of the outburst decay, with softening emission as the flux decayed, and the non-thermal soft X-ray spectral component fading faster than the thermal one. Almost simultaneously to our second and fourth *XMM-Newton* observations (on 2008 August 29 and September 2), we observed the source in the hard X-ray range with *INTEGRAL*, which clearly detected the source up to ~ 100 keV in the first pointing, while giving only upper limits during the second pointing, discovering a variable hard X-ray component fading in less than 10 days after the bursting activation. We performed a phase-coherent X-ray timing analysis over about 160 days starting with the burst activation and found evidence of a strong second derivative period component ($\ddot{P} = -1.6(4) \times 10^{-19} \text{ s s}^{-2}$). Thanks to the phase-connection, we were able to study the the phase-resolved spectral evolution of SGR 0501+4516 in great detail. We also report on the *ROSAT* quiescent source data, taken back in 1992 when the source exhibits a flux ~ 80 times lower than that measured during the outburst, and a rather soft, thermal spectrum.

Key words: stars: pulsars: general — pulsar: individual: SGR 0501+4516

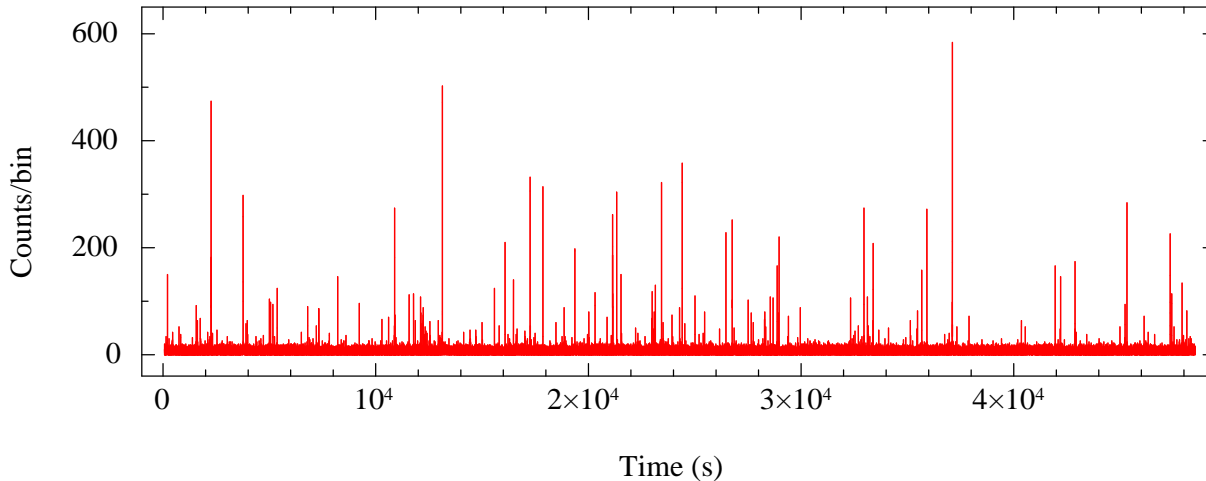


Figure 1. EPIC-pn lightcurve (binned at 0.5 s) of the 2008 August 23rd observation. Times are in seconds from: MJD 54701 01:07:32 (UT).

1 INTRODUCTION

Over the last few years, a number of observational discoveries have placed “magnetars” (ultra-magnetized isolated neutron stars) in the limelight again. These extreme objects comprise the Anomalous X-ray Pulsars (AXPs; 10 objects), and the Soft Gamma-ray Repeaters (SGRs; 4 objects), which are observationally very similar classes in many respects (for a recent review see Mereghetti et al. 2008). They are all slow X-ray pulsars with spin periods clustered in a narrow range ($P \sim 2\text{--}12$ s), relatively large period derivatives ($\dot{P} \sim 10^{-13} - 10^{-10} \text{ s s}^{-1}$), spin-down ages of $10^3 - 10^4$ yr, and magnetic fields, as inferred from the classical magnetic dipole spin-down formula, of $10^{14} - 10^{15}$ G, much higher than the electron quantum critical field ($B_{cr} \simeq 4.4 \times 10^{13}$ G). About a dozen AXPs and SGRs are strong persistent X-ray emitters, with X-ray luminosities of about $10^{34} - 10^{36} \text{ erg s}^{-1}$, and a few transient ones have been discovered in recent years. A peculiarity of these neutron stars is that their X-ray energy output is much larger than their rotational energy losses, so they can not be only rotationally powered. Furthermore, they lack a companion, so they can not be accretion-powered either. Rather, the powering mechanism of AXPs and SGRs is believed to reside in the neutron star ultra-strong magnetic field (Duncan & Thompson 1992; Thompson & Duncan 1993). Other scenarios, beside the “magnetar” model, were proposed to explain AXP and SGR emission, such as the fossil disk (Chatterjee, Hernquist & Narayan 2000; Perna, Hernquist, & Narayan 2000) and the quark-star model (Ouyed, Leahy, & Niebergal 2007a,b).

In the 0.1–10 keV energy band, magnetars spectra are relatively soft and empirically modeled by an absorbed blackbody ($kT \sim 0.2\text{--}0.6$ keV) plus a power-law ($\Gamma \sim 2\text{--}4$). Thanks to *INTEGRAL*–ISGRI and *RXTE*–HEXTE, hard X-ray emission up to ~ 200 keV has recently been detected from some sources (Kuiper et al. 2004, 2006; Mereghetti et al. 2005; Götz et al. 2006). This discovery has opened a new window on magnetars studies and has shown that their energy output may be dominated by hard, rather than soft emission.

At variance with other isolated neutron stars, AXPs and

SGRs exhibit spectacular episodes of bursting and flaring activity, during which their luminosity may change up to 10 orders of magnitude on timescales down to few milliseconds. Different types of X-ray flux variability have been observed, ranging from slow and moderate flux changes up to a factor of a few on timescales of years (shown by virtually all members of the class), to more intense outbursts with flux variations up to ~ 100 lasting for $\sim 1\text{--}3$ years, and to short and intense X-ray burst activity on sub-second timescales (see Kaspi 2007 and Mereghetti 2008 for reviews of X-ray variability).

In particular, SGRs are characterized by periods of activity during which they emit numerous *short bursts* in the hard X-ray / soft gamma-ray energy range ($t \sim 0.1 - 0.2$ s; $L \sim 10^{38} - 10^{41}$ erg/s). This is indeed the defining property that led to the discovery of this class of sources. In addition, they have been observed to emit *intermediate flares*, with typical durations of $t \sim 1 - 60$ s and luminosities of $L \sim 10^{41} - 10^{43}$ erg/s, and spectacular *Giant Flares*. The latter are rare and unique events in the X-ray sky, by far the most energetic ($\sim 10^{44} - 10^{47}$ erg/s) Galactic events currently known, second only to Supernova explosions. Indeed, the idea that SGRs host an ultra-magnetized neutron star was originally proposed to explain the very extreme properties of their bursts and flares: in this model the frequent short bursts are associated with small cracks in the neutron star crust, driven by magnetic diffusion, or, alternatively, with the sudden loss of magnetic equilibrium through the development of a tearing instability, while the giant flares would be linked to global rearrangements of the magnetic field in the neutron stars magnetosphere and interior (Thompson & Duncan 1995; Lyutikov 2003).

Bursts and flares do not seem to repeat with any regular, predictable pattern. Giant flares have been so far observed only three times from the whole sample of SGRs (from SGR 0526–66 in 1979, Mazets et al. 1979; from SGR 1806–20 in 1998, Hurley et al. 1999; and from SGR 1900+14 in 2004, e.g. Hurley et al. 2005, Palmer et al. 2005), and never twice from the same source. As far as short bursts and intermediate flares are concerned, while some SGRs (such as SGR 1806–20) are extremely active sources,

Parameters	2008-08-23	2008-08-29	2008-08-31	2008-09-02	2008-09-30
Start (UT)	01:07:36	07:10:28	12:09:45	10:00:38	02:18:44
End (UT)	14:35:33	13:58:20	14:59:58	15:41:49	11:22:15
Exposure (ks)	48.9	24.9	10.2	20.5	31.0
Counts/s (pn)	8.520 ± 0.016	7.08 ± 0.02	6.60 ± 0.03	6.05 ± 0.02	3.23 ± 0.01
Pulse Period (s)	5.7620694(1)	5.7620730(1)	5.7620742(1)	5.7620754(1)	5.7620917(1)
Pulsed Fraction (%)	41(1)	35(1)	38(1)	38(1)	43(1)
N. bursts	80	2	0	0	0

Table 1. *Top table:* Summary of the first 5 *XMM-Newton* observations of SGR 0501+4516. The exposure time refers to the pn camera. Count-rates are background-corrected, and refers to the pn in Small Window, except for the last observation which was in Large Window. *Bottom table:* Timing properties of SGR 0501+4516. The pulsed fraction is defined as the background-corrected $(max-min)/(max+min)$ in the 0.3-12keV energy band. The number of bursts refers to spikes detected at >35 count/s.

in other cases no bursts have been detected for many years (as in the case of SGR 1627-41, that re-activated in May 2008 after a 10-yr long stretch of quiescence; Esposito et al. 2008). This suggests that a relatively large number of members of this class has not been discovered yet, and may manifest themselves in the future.

On 2008 August 22, a new SGR, namely SGR 0501+4516, was discovered (the first in ten years), thanks to the *Swift*-BAT detection of a series of short X-ray bursts and intermediate flares (Holland et al. 2008; Barthelmy et al. 2008). X-ray pulsations were observed by *RXTE* at a period of 5.7s, confirming the magnetar nature of this source (Gögüş et al. 2008), and its counterpart was identified in the infrared and optical bands (Tanvir et al. 2008; Rea et al. 2008b; Fatkhullin et al. 2008; Rol et al. 2008). Prompt radio observations to search for the on-set of radio pulsation and of a persistent counterpart failed to reveal any emission in this band in the first days after the outburst activation (Hessels et al. 2008; Kulkarni & Frail 2008b; Gelfand et al. 2008).

In this paper, we present a series of 5 *XMM-Newton* observations of SGR 0501+4516; the first one was performed only 1 day after the SGR activation, and the last one after 38 days. We also report on two *INTEGRAL* observations; the first was performed almost simultaneously with the second *XMM-Newton* observation, while the other one was performed soon after the fourth *XMM-Newton* pointing. We used the *Swift*-XRT monitoring to model the outburst decay and the spin period evolution of the source until ~ 160 days after the onset of the bursting activity. We also report on the 1992 *ROSAT* observation of its quiescent counterpart. We present details of the observation and analysis in § 2, and results in § 3 and 4. Discussion follows in § 5.

2 OBSERVATIONS AND ANALYSIS

2.1 XMM-Newton

The *XMM-Newton* Observatory (Jansen et al. 2001) observed SGR 0501+4516 on August/September 2008 (see Tab.1) with the EPIC instruments (pn and MOSs; Turner et al. 2001; Strüder et al. 2001), the Reflecting Grating Spectrometer (RGS; den Herder et al. 2001), and the Optical Monitor (OM; Mason et al. 2001).

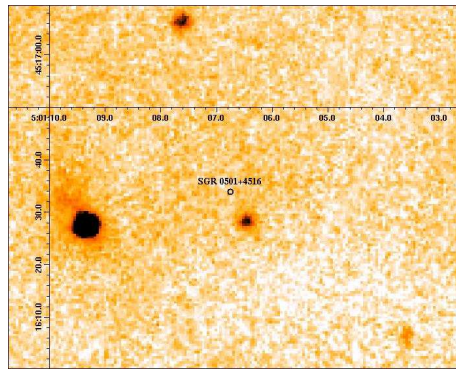


Figure 2. Co-added image of all the OM observations in the UVW1 filter. The four bright objects are USNO B1 stars.

Data were processed using SAS version 7.1.0 with the most up to date calibration files (CCF) available at the time the reduction was performed (October 2008). Standard data screening criteria were applied in the extraction of scientific products. Soft proton flares were not observed in any of the observations, resulting in the total on-source exposure times listed in Tab 1.

2.1.1 EPIC and RGS

For four of the observations the pn camera was set in **Small Window** mode in order to reduce pile-up, while for the 2008 September 30th observation it was in **Large Window** mode. The MOS1 camera was in **Full Frame** for the first observation, and in **Small Window** for all the other pointings. On the other hand, the MOS2 was in **Timing** mode, except for the last observation where it was set in **Small Window** mode. All other MOS CCDs were in **Prime Full Window** mode. Thick filters were used for all the instruments, and pile-up was present only in the first MOS1 observation, which we ignored in the rest of the analysis. No transients were present in any imaging camera, so we are confident that the MOS2 in non-imaging mode did not collect photons from anything else than our target.

We performed a 2-dimensional or 1-dimensional PSF fitting, for the data obtained with the EPIC cameras in imaging mode or timing mode, respectively. The extraction radius was chosen in such a way as to obtain more than 90% of the source counts.

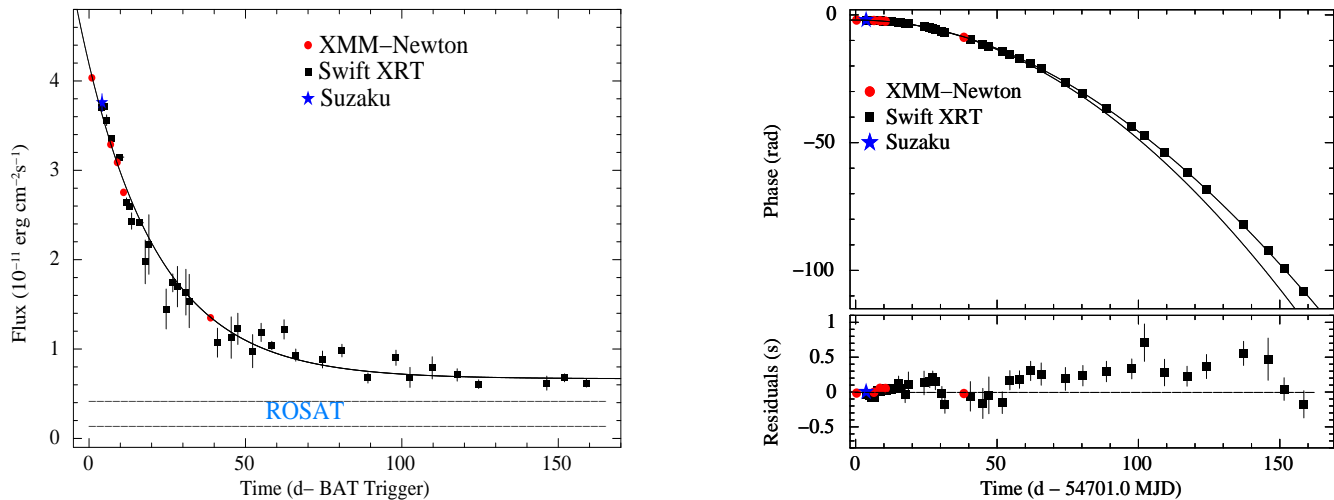


Figure 3. *Left hand panel:* the outburst decay of the persistent X-ray flux of SGR 0501+4516 fitted with an exponential function (see §5 for details). We refer here as BAT trigger: MJD 54700.0 12:41:59.000 (UT). The fluxes are absorbed and in the 1–10 keV energy range for *XMM-Newton*, *Swift*, and *Suzaku* (Enoto et al. 2009), while the *ROSAT* flux is extrapolated to the same band, and refers to two different spectral models (see §4 for details). *Right hand panel:* The 0.5–10 keV pulse phase evolution with time, together with the time residuals with respect to the phase coherent timing solution discussed in the text and including $P/\dot{P}/\ddot{P}$ components. The solid lines in the upper panel represent the timing solution with (top line) and without (low line) the cubic term.

We then extracted the source photons, for the cameras set-up in imaging mode, from a circular region with $30''$ radius, centered at the source position (RA 05:01:06.607, Dec +45:16:33.47 at J2000, with a 1σ error of $1''.5$ which refers to the absolute astrometric *XMM-Newton* accuracy (Kirsh et al. 2004))¹. The background was obtained from a similar region as far away as possible from the source location in the same CCD. For the MOS2 camera in timing mode we extracted the photons from RAWX 274-334, and a similar region was used for the background extraction, although as far as possible from the source position. Only photons with $\text{PATTERN} \leq 4$ were used for the pn, with $\text{PATTERN} \leq 12$ for the MOS2 when in imaging mode, and with $\text{PATTERN} = 0$ were used for MOS2 observations in timing mode. All the photon arrival times have been corrected to refer to the barycenter of the Solar System.

Thanks to the high timing and spectral resolution² of the pn and MOS cameras, and to the high spectroscopic accuracy of the RGS, we were able to perform timing and spectral analysis, as well as pulse phase spectroscopy. Both the MOSs and pn cameras gave consistent timing and spectral results, and we report only on the pn results (see Tab. 1 for the pn source count rates for all five observations), and the RGS is used only to constrain the presence of narrow lines (see §4).

For the timing (§3) and spectral analysis (§4) we removed the bursts observed in the first two observations (August 23rd and 29th) discarding all the photons corresponding to intervals where the source count rate exceeded 35

counts s^{-1} (a detailed analysis of the bursts themselves will be reported elsewhere).

2.1.2 Optical Monitor

Twenty five OM images of the field were obtained simultaneously to the X-ray observations through the UVW1 lenticular filter. One further image was obtained through the U filter. The UVW1 has an effective transmission range of $\lambda = 2410\text{--}3565$ Å, peak efficiency at $\lambda = 2675$ Å, full-width half-maximum image resolution of $2''$ and a Vega-spectrum zeropoint of $m = 17.20$. The U has an effective transmission range of $\lambda = 3030\text{--}3890$ Å, peak efficiency at $\lambda = 3275$ Å, full-width half-maximum image resolution of $1.55''$ and a Vega-spectrum zeropoint of $m = 18.26$. Modulo-8 fixed photon pattern and scattered background light were removed from individual images before correcting optical distortion and converting images to J2000 celestial coordinates. The *XMM-Newton* star trackers provide absolute pointing accuracy to $1''.8$. To refine astrometry, a correction is performed to individual images by cross-correlating source positions in the OM with counterparts in the USNO-B1.0 catalogue (Monet 2003). The UVW1 images were mosaicked to produce a 70 ks summed exposure. The U band image was accumulated over an exposure time of 4 ks. Aperture photometry was performed on the source position of SGR 0501+4516 using a standard $17''.5$ radius circular aperture for the UVW1 image and $3''$ for the U image, consistent with the calibrated zeropoint.

No XMM-OM source is detected within this aperture to 3σ magnitude upper limits of $m_U > 22.1$ and $m_{\text{UVW1}} > 23.7$ (see Fig. 2). We also searched for possible counterparts to the X-ray bursts in the XMM-OM exposures in the UVW1

¹ Consistent with the more accurate *Chandra* determination: RA 05:01:06.756, Dec +45:16:33.92 ($0.11''$ error circle; Woods et al. 2008)

² see <http://xmm.esac.esa.int/> for details.

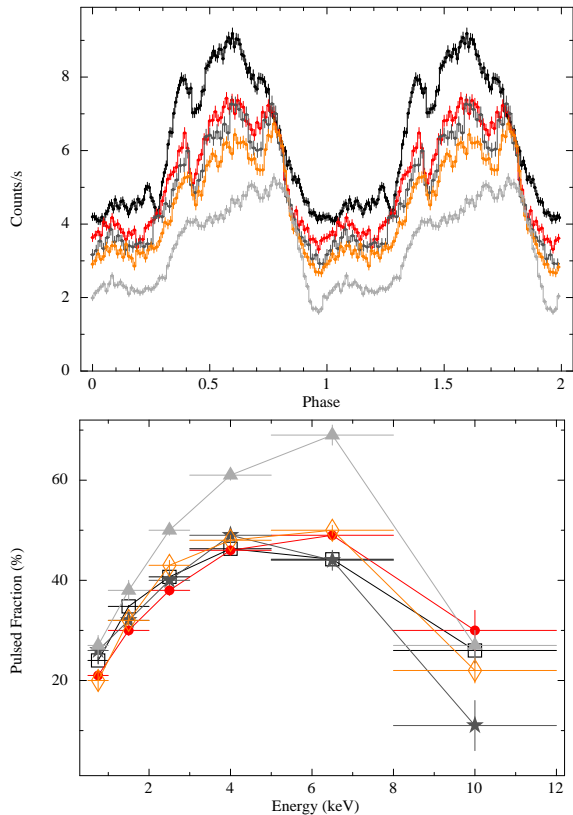


Figure 4. *Top panel:* Pulse profiles of the 5 *XMM-Newton* observations in the 0.3–12 keV energy band. *Bottom panel:* Pulsed fraction dependence with energy for the same observations. In both panels the black, red, dark grey, orange and light grey colors refer to the five observations ordered by increasing epoch.

filter during the first *XMM-Newton* observation. We did not find any signature for such bursts in the UVW1 filter with a 3σ upper limit on each 4 ks image of $m_{UVW1} > 22.05$.

2.2 INTEGRAL

INTEGRAL (Winkler et al. 2003) observed SGR 0501+4516 twice, soon after its discovery: the first observation (orbit 717), soon after its discovery, started on 2008 August 27 at 00:31 (UT) as a ToO observation (ending on August 28th 08:36 UT), and the second observation in the framework of the Core Programme observations of the Perseus Arm region starting on 2008 September 5 at 05:48, and ending at 07:40 (UT) on September 10th (orbits 720 and 721). We analyzed the IBIS/ISGRI data of both observations. IBIS (Ubertini et al. 2003) is a coded mask telescope with a wide ($29^\circ \times 29^\circ$) field of view, sensitive in the 15 keV–10 MeV energy range. We restricted our analysis to the ISGRI (Lebrun et al. 2003) data, taken by the IBIS low energy (15 keV–1 MeV) CdTe detector layer, since ISGRI the most sensitive instrument on board *INTEGRAL* at energies < 300 keV.

For the first observation an effective exposure of 204 ks was accumulated at the source position. During this observation, the source was still burst-active and indeed at least 4 weak bursts were detected in the ISGRI data (Hurley et al. 2008). In the 18–60 keV image the source is detected at a $\sim 4.2\sigma$ confidence level, corresponding to a count

rate of 0.31 ± 0.08 counts s^{-1} , while in the 60–100 keV band the source was detected at a ~ 3.5 sigma level (0.25 ± 0.07 counts s^{-1}). Above 100 keV the source is not detected and the 3σ upper limit is 0.2 counts s^{-1} (100–200 keV). The ISGRI response matrices were rebinned to match the above two channels and the detected flux values were used in the broad band spectral analysis (see below §4).

We performed the same analysis on the Core Programme data. In this case the exposure time was 361 ks at the position of the source. No persistent or burst emission was detected in this second observation. We could infer a 3σ upper limit in the 18–60 keV energy band of 0.18 counts s^{-1} , implying a decrease of the hard X-ray flux in about 10 days of a factor of ~ 2 .

2.3 Swift-XRT

The *Swift* satellite (Gehrels et al. 2004) includes a wide-field instrument, the Burst Alert Telescope (BAT; Barthelmy et al. 2005), and two narrow-field instruments, the X-Ray Telescope (XRT; Burrows et al. 2005) and the Ultraviolet/Optical Telescope (UVOT; Roming et al. 2005), and discovered the bursting activity of SGR 0501+4516 thanks to the large field of view of the BAT camera (Holland et al. 2008; Barthelmy et al. 2008). We briefly report here on the *Swift*-XRT monitoring of SGR 0501+4516, and we refer to Palmer et al. and Göğüş et al. (2009, in preparation) for further details on the *Swift* observations.

Starting a few hours after the burst activation, the *Swift*-XRT camera monitored SGR 0501+4516, collecting a few tens of observations in the following 160 days. The XRT instrument was operated in photon counting (PC) mode for the first two observations, and in window timing (WT) mode for all the following observations, which ensures enough timing resolution (1.766 ms) to monitor the period changes of the source. In our analysis we ignored the first two observations in PC mode because they were highly affected by photon pile-up.

The data were processed with standard procedures using the *FTOOLS* task *XRTPIPELINE* (version 0.12.0) and events with grades 0–2 were selected for the WT data. For the timing and spectral analysis, we extracted events in a region of 40×40 pixels. To estimate the background, we extracted the WT events within a similar box far from the target. The event files were used to study the timing properties of the pulsar after correcting the photon arrival times to the barycenter of the Solar System. For the spectral fitting (aimed at having a reliable flux measurement over the entire outburst) the data were grouped so as to have at least 20 counts per energy bin. The ancillary response files were generated with *XRTMKARF*, and they account for different extraction regions, vignetting and point-spread function corrections. We used the latest available spectral redistribution matrix (v011) in *CALDB*. We removed the bursts from the XRT observations taking out all the photons corresponding to intervals where the source count rate exceeded 5 counts s^{-1} .

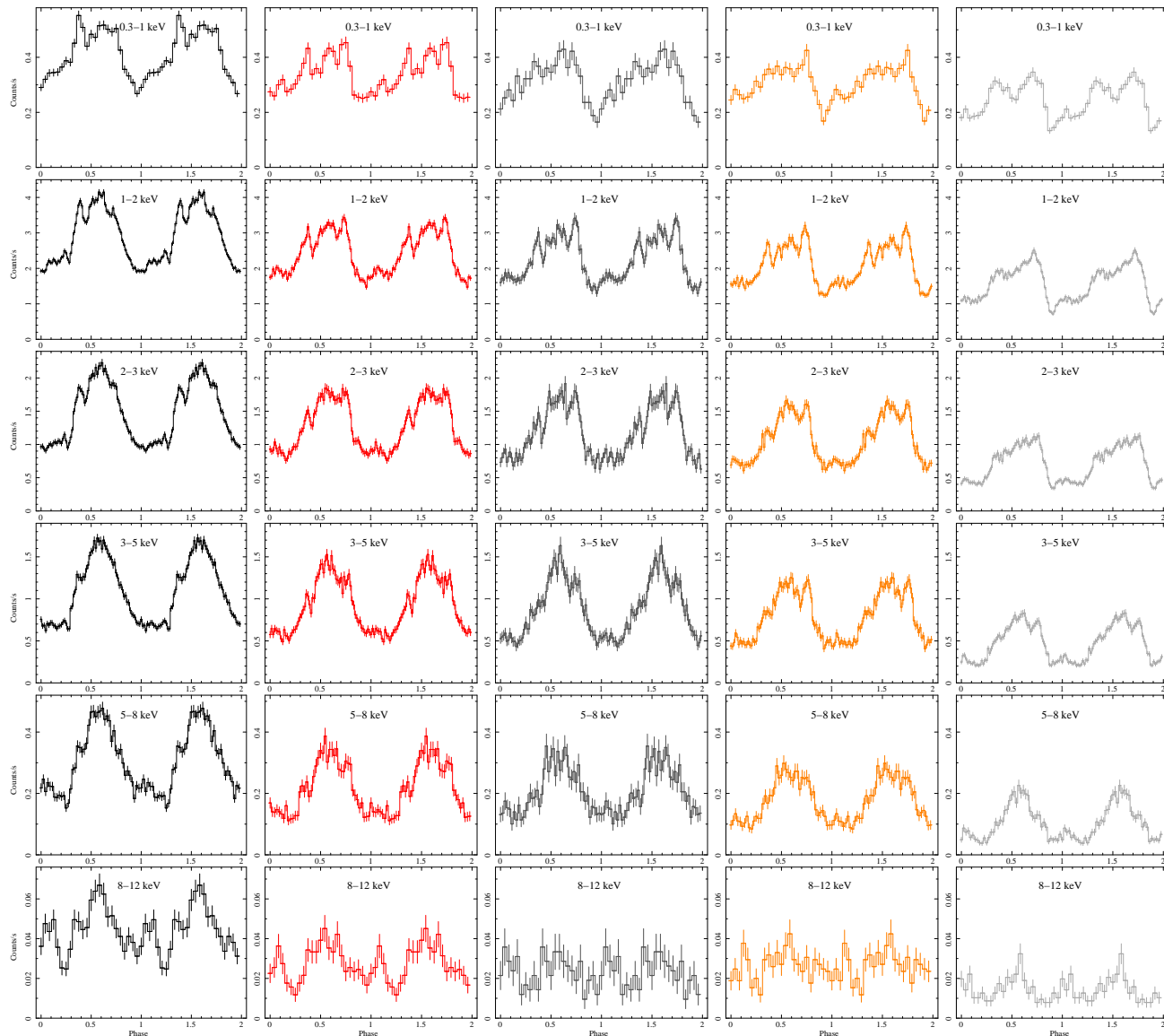


Figure 5. Pulse profiles (phase vs counts/s) as a function of energy for all five *XMM-Newton* observations of SGR 0501+4516. Each column displays one *XMM-Newton* observation with epoch increasing from left to right.

2.4 ROSAT

The *Röntgensatellit* (ROSAT; Voges 1992; Snowden & Schmitt 1990) Position Sensitive Proportional Counter (PSPC) serendipitously observed the region of the sky including the position of SGR 0501+4516 between 1992 September 21 and 24, for an effective exposure time of 4.2 ks. An off-axis point source, 2RXP J050107.7+451637, was clearly detected in the observation, the position of which is consistent, within uncertainties, with that of SGR 0501+4516 as inferred by *Chandra* (Woods et al. 2008).

The ROSAT event list and spectrum of 2RXP J050107.7+451637 included about 260 background-subtracted photons accumulated from a circle of about 1.7 radius (corresponding to an encircled energy of $\sim 90\%$). The source count rate is estimated to be $(6.6 \pm 0.5) \times 10^{-2}$ counts s^{-1} after correction for the point-spread function and vignetting.

3 X-RAY TIMING ANALYSIS

We started the timing analysis by performing a power spectrum of the first *XMM-Newton* observation (after having cleaned the data for the bursts; see above), and we found a strong coherent signal at ~ 5.76 s, followed by 8 significant harmonics. We then refined our period measurement studying the phase evolution within the observation by means of a phase-fitting technique (see Dall’Osso et al. 2003 for details). The resulting best-fit period is $P = 5.762070(3)$ s (1σ confidence level; epoch 54701.0 MJD). The accuracy of $3\mu s$ is enough to phase-connect coherently the first two *XMM-Newton* pointings which are about 6 days apart. The procedure was repeated by adding, each time, a single *XMM-Newton* pointing. The relative phases were such that the signal phase evolution could be followed unambiguously in the 5 *XMM-Newton* observations, and the preliminary phase-coherent solution for these observations had a best-fit period

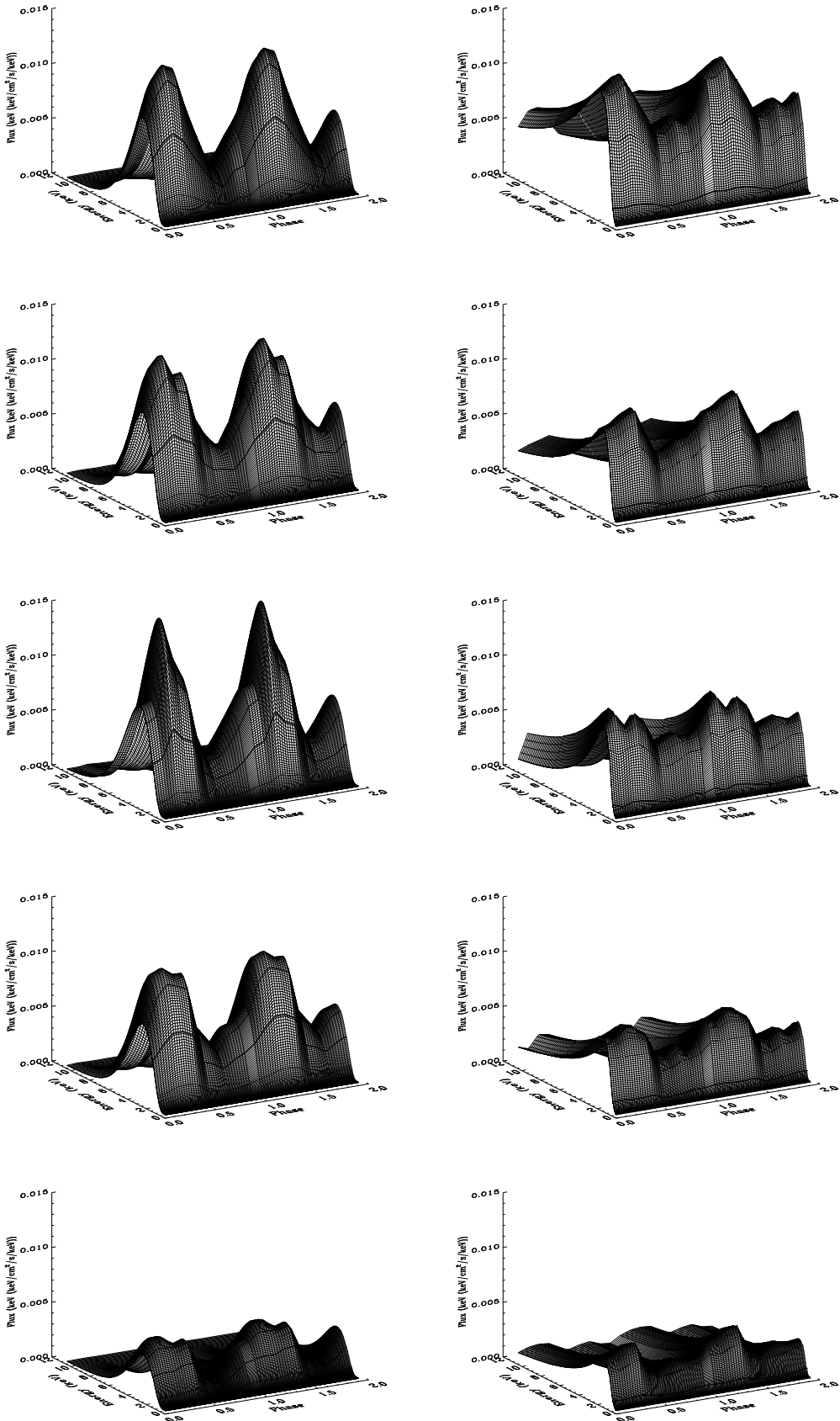


Figure 6. 3D pulse profiles for the five *XMM-Newton* observations of SGR 0501+4516 (the epoch increases from top row to bottom row). *Left column:* pulse profiles of the BB component as a function of the energy. *Right column:* pulse profiles of the PL component as a function of the energy.

Parameters	Blackbody + Power-law				
	2008-08-23	2008-08-29	2008-08-31	2008-09-02	2008-09-30
kT (keV)	0.70 ± 0.01	0.69 ± 0.01	0.70 ± 0.01	0.69 ± 0.01	0.66 ± 0.01
BB Radius (km)	1.41 ± 0.05	1.49 ± 0.05	1.42 ± 0.06	1.39 ± 0.04	1.04 ± 0.06
BB flux	2.1 ± 0.1	2.3 ± 0.1	2.15 ± 0.13	1.93 ± 0.07	0.86 ± 0.11
Γ	2.75 ± 0.02	2.92 ± 0.04	2.90 ± 0.06	2.96 ± 0.08	3.01 ± 0.04
PL flux	7.7 ± 0.1	5.8 ± 0.1	5.3 ± 0.2	4.9 ± 0.2	3.3 ± 0.1
Abs. Flux	4.1 ± 0.1	3.4 ± 0.2	3.14 ± 0.23	2.8 ± 0.1	1.4 ± 0.1
Unab. Flux	9.6 ± 0.1	8.1 ± 0.2	7.5 ± 0.3	7.0 ± 0.3	4.17 ± 0.11

Table 2. Parameters for the spectral modelling of the phase-averaged spectrum of SGR 0501+4516 with an absorbed blackbody plus a power-law (χ^2_{ν} (d.o.f.) = 1.14 (838)), for all five *XMM-Newton* observations. The N_H value is $(0.89 \pm 0.01) \times 10^{22} \text{ cm}^{-2}$ with solar abundances from Anders & Grevesse (1989). The blackbody radius is calculated at infinity, and assuming a distance of 5 kpc (note that in the error calculation we did not consider the uncertainty in the distance). Unless otherwise specified, all fluxes are unabsorbed, in the 0.5-10 keV range, and in units of $10^{-11} \text{ erg cm}^{-2} \text{ s}^{-1}$. Errors are at the 90% confidence level.

of $P = 5.7620692(2) \text{ s}$ and $\dot{P} = 6.8(8) \times 10^{-12} \text{ s s}^{-1}$ (MJD 54701.0 was used as reference epoch; $\chi^2 \sim 4$ for 3 degrees of freedom, hereafter d.o.f.).

To better sample the pulsations in the time intervals not covered by *XMM-Newton* data, and increase the accuracy of our timing solution, we also included the *Suzaku*-XIS observation (Enoto et al. 2009) and part of the *Swift*-XRT monitoring dataset. A quadratic term in the phase evolution is required starting about one month after the *Swift*-BAT onset, when the pulse phases increasingly deviate from the extrapolation of the above $P-\dot{P}$ solution (see Fig. 3), resulting in an unacceptable fit ($\chi^2 \sim 110$ for 16 d.o.f.). Therefore, we added a higher order component to the above solution to account for the possible presence of a temporary or secular \ddot{P} term. The resulting new phase-coherent solution had a best-fit for $P = 5.7620695(1) \text{ s}$, $\dot{P} = 6.7(1) \times 10^{-12} \text{ s s}^{-1}$, and $\ddot{P} = -1.6(4) \times 10^{-19} \text{ s s}^{-2}$ (MJD 54701.0 was used as reference epoch; 1σ c.l.; $\chi^2 = 58$ for 45 d.o.f.), or $\nu = 0.173548754(4) \text{ Hz}$, $\dot{\nu} = -2.01(3) \times 10^{-13} \text{ Hz s}^{-1}$, and $\ddot{\nu} = 5(1) \times 10^{-21} \text{ Hz s}^{-2}$. The time residuals with respect to the new timing solution are reported in Fig. 3 (central panel; empty squares). The significance of the inclusion of the cubic term is 5.3σ . Moreover, the new timing solution implies a root mean square variability of only 0.04 s. We note that the new timing solution is in agreement with that reported by Israel et al. (2008a).

The negative sign of \ddot{P} implies that the spin-down is decreasing on a characteristic timescale of about half a year. This might imply that a transient increase of the spin-down above the secular trend occurred in connection with the outburst onset, and that the source might now be recovering toward its secular spin-down. We note that timing components of similar strengths and with similar evolution timescales were detected in other AXPs and SGRs following the occurrence of glitches (Dall’Osso et al. 2003; Dib et al. 2008). This finding suggests that a similar event might have occurred connected to the burst and/or outburst behavior displayed by SGR 0501+4516 in August 2008. Correspondingly, assuming that the secular spin-down was an order of magnitude smaller than the one we measured during the outburst, our findings imply a magnetic field strength of the dipolar

component in the range $7 \times 10^{13} < B_d < 2 \times 10^{14} \text{ Gauss}$ (assuming a neutron star moment of inertia of 10^{45} g cm^2).

The 0.3-11 keV SGR 0501+4516 pulse profiles are relatively complex, with several sub-peaks, though dominated by the sinusoidal fundamental component (see Fig. 4 and top panels of Fig. 9). The fundamental pulsed fraction calculated as $(\text{max} - \text{min})/(\text{max} + \text{min})$ is fairly constant in time (although with some oscillations) changing from $41\% \pm 1\%$ during the first *XMM-Newton* pointing, to $35\% \pm 1\%$ (2nd pointing), to $38\% \pm 1\%$ (3rd and 4th pointings), and finally to $43\% \pm 1\%$ (last pointing; see also Tab. 1). At the same time both the shape and the pulsed fraction change as a function of energy within each pointing (see Fig. 5 and Fig. 6).

The *ROSAT* photon arrival times were corrected to the barycenter of the Solar System and a search for coherent periodicities was performed in a narrow range of trial periods (6.1–5.5 s; we assumed a conservative value of $|\dot{P}| = 6 \times 10^{-10} \text{ s s}^{-1}$) centered around the 2008 August period. No significant peaks were found above the 3σ detection threshold. The corresponding upper limit to the pulsed fraction is about 50%.

4 SPECTRAL ANALYSIS

For the spectral analysis we used source and background photons extracted as described in §2. The response matrices were built using ad-hoc bad-pixel files built for each observation. We use the *XSPEC* package (version 11.3, and as a further check also the 12.1) for all fittings, and used the *phabs* absorption model with the Anders & Grevesse (1989) solar abundances and Balucinska-Church & McCammon (1998) photoelectric cross-sections. We restricted our spectral modeling to the EPIC-pn camera and used only the best calibrated energy range³, namely 0.5–10 keV.

³ Note that in all our fittings there is a weak spurious absorption feature at $\sim 2.2 \text{ keV}$, which is of instrumental nature, and due to the Au edge.

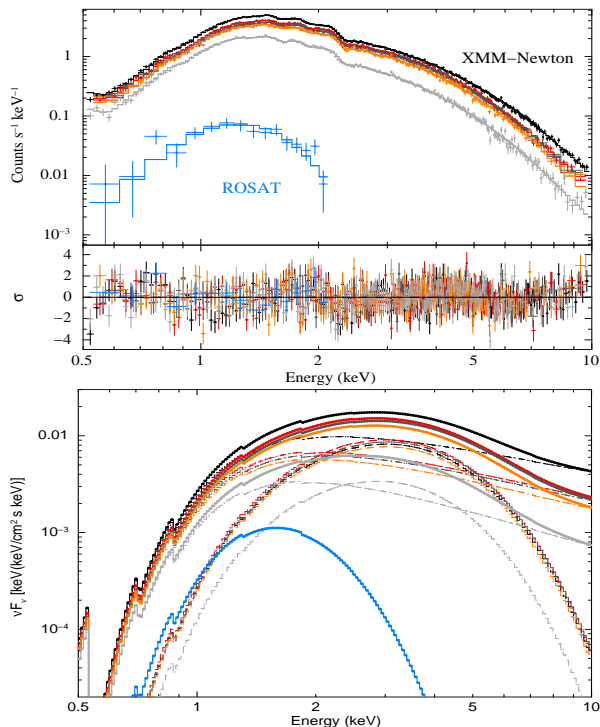


Figure 7. Phase-averaged spectra and νF_ν plot of the fitted models for the five *XMM-Newton* observations (again the black, red, dark grey, orange and light grey colors refer to the five observations ordered by increasing epoch) and the quiescent *ROSAT* counterpart (in blue).

4.1 Phase-averaged spectroscopy

We started the spectral analysis by fitting simultaneously the spectra of all the *XMM-Newton* observations with the standard blackbody (BB) plus power-law (PL) model, leaving all parameters free to vary except for the N_H which was constrained to be the same in all observations. The values for the simultaneous modeling are reported in Tab. 2, with a final reduced $\chi^2_\nu = 1.14$ for 838 d.o.f. (see also Fig. 7). The values of the spectral parameters were not significantly different when modelling each observation separately. The measured hydrogen column density is $N_H = 0.89 \times 10^{22} \text{ cm}^{-2}$, and the absorbed flux in the 0.5–10 keV band varied from 4.1 to $1.4 \times 10^{-11} \text{ erg s}^{-1} \text{ cm}^{-2}$, corresponding to a luminosity range of 1.2 to $0.42 \times 10^{35} d_5^2 \text{ erg s}^{-1}$ (where d_5 is the source distance in units of 5 kpc; see § 5.1 for further discussion on the source distance).

In the 0.5–10 keV band, the blackbody component accounts for $\sim 15\%$ of the total absorbed flux throughout the outburst. The blackbody radius, as derived from its normalization, is smaller than the neutron star size, being compatible with a constant of ~ 1.4 km during the first month of the outburst decay (although hints for a decrease can be seen in the last observation). If the blackbody emission originates from the star surface this would imply that only a small fraction of the surface is emitting.

There is evidence that as the flux decreased, the 0.5–10 keV spectrum softened during the first month after the bursting activation (see Tab. 2 and Fig. 7). Interestingly, the BB flux decreased much slower than the PL flux, remaining almost constant for the first 10 days, and significantly

decreasing only in the last observation more than a month after the burst activation (see also § 5, Fig. 6 and Fig. 7).

Since the *INTEGRAL* observation of SGR 0501+4516 was almost simultaneous to our second *XMM-Newton* observation, we then extended our spectral modelling to the entire 0.5–100 keV spectrum of the 2008 August 29 observation. We found that the BB+PL model was no longer statistically acceptable ($\chi^2_\nu = 1.29$ for 174 d.o.f.), and that the PL used to model the soft X-ray spectrum could not account for the emission above 10 keV (as it is usually the case for SGRs; Götz et al. 2006). We then tried more complex models. In line with other magnetar spectra (Kuiper et al. 2006; Götz et al. 2006), we added a second PL to the data to account for the hard X-ray emission. The results are reported in Tab. 3 (see also Fig. 8), where we also report the F-test probability for the addition of a further component to the fit. We also note that an excess in the residuals at energies larger than 8 keV was present in the first *XMM-Newton* observation when fit with a BB+PL model (see Fig. 7), probably due to the presence of the same hard X-ray component detected by *INTEGRAL*, which might have been present from the beginning of the outburst. The subsequent *INTEGRAL* observation close to the fourth *XMM-Newton* observation almost a week later, did not show any hard X-ray emission. Assuming (although unlikely) that the hard X-ray spectral index did not change during the flux decay, we can translate our non-detection in a 3σ flux upper limit in the 18–60 keV band of $< 9.7 \times 10^{-12} \text{ erg s}^{-1}$.

To take into account the presence of this hard X-ray component we also fit the first *XMM-Newton* observation with a BB plus two PLs, fixing the power-law index of the hard PL at the value inferred from the *XMM-Newton* plus *INTEGRAL* modelling of the second observation (namely $\Gamma = 0.8$; see the first and second columns of Tab. 3). The addition of this component was barely significant, less than in the 2008 August 29, although in the latter case the *INTEGRAL* data were crucial in the spectral modeling. We similarly tried to model the third *XMM-Newton* observation adding this PL component but in this case the addition of this further component was not significant. As in the case of the soft X-ray component, we found that the hard X-ray flux decreased significantly during the outburst decay, being undetectable by *INTEGRAL* only 10 days after the burst activation.

Simultaneously with the second *INTEGRAL* observation, an *AGILE* observation was reported in the energy range > 100 MeV, starting on August 31st and ending on September 10th (Feroci et al. 2008). During the *AGILE* observation the source was marginally burst-active. The *AGILE*-GRID gamma-ray experiment did not detect the source, with a reported 2σ upper limit of $13 \times 10^{-8} \text{ photon cm}^{-2} \text{ s}^{-1}$. Assuming an average photon energy of 500 MeV, this value corresponds to $\sim 6 \times 10^{-2} \text{ keV (keV cm}^{-2} \text{ s}^{-1} \text{ keV}^{-1})$, well below the extrapolation at this energy of the *INTEGRAL* power-law detected during the August 29th observation (prior to the *AGILE* observation), that would predict a flux at 500 MeV of $\sim 10^3 \text{ keV (keV cm}^{-2} \text{ s}^{-1} \text{ keV}^{-1})$. This indicates that as in the AXP cases (Kuiper et al. 2006), also in this SGR the presence of a spectral cut-off at energies between 100 keV and 100 MeV should be present spectrum during outburst.

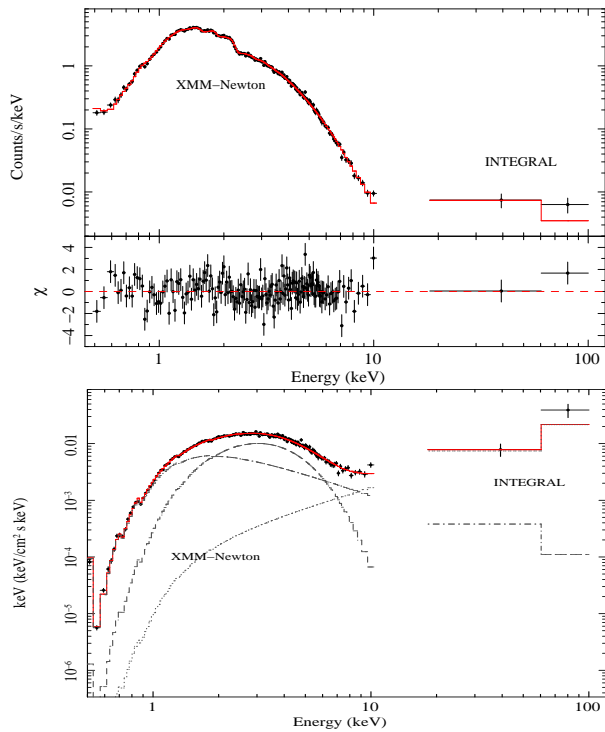


Figure 8. Phase-averaged spectra of the second *XMM-Newton* observation and the quasi-simultaneous *INTEGRAL* one, modelled with a blackbody plus two power-laws (see also Tab. 3).

We then studied the pre-outburst quiescent spectrum of SGR 0501+4516 as observed by *ROSAT*. The quiescent spectrum was well fit by either a BB or PL single-component model (see Fig. 7). The best-fit parameters are $N_H = 6_{-3}^{+5} \times 10^{21} \text{ cm}^{-2}$ and $kT = 0.38_{-0.15}^{+0.36} \text{ keV}$ for the BB, and $N_H = 8_{-4}^{+11} \times 10^{21} \text{ cm}^{-2}$ and $\Gamma > 0.6$ for the PL (reduced $\chi^2 = 1.08$ and $\chi^2 = 1.13$ for 17 d.o.f., respectively). The 0.1–2.4 keV observed flux is $F_X \sim 1.4 \times 10^{-12} \text{ erg cm}^{-2} \text{ s}^{-1}$, corresponding to an extrapolated 1–10 keV fluxes of 1.3 and $4.2 \times 10^{-12} \text{ erg cm}^{-2} \text{ s}^{-1}$ for the BB and PL models, respectively. In analogy with the quiescent spectra of other magnetars, and given the slightly better reduced χ^2 we assume that the BB spectral modeling is more correct.

No spectral features were detected in the phase-averaged *XMM-Newton* spectra, with 3σ upper limits to the equivalent width of 45 and 65 eV, for a Gaussian absorption line with $\sigma_{\text{line}} = 5 \text{ eV}$ (using the RGS spectra) and $\sigma_{\text{line}} = 100 \text{ eV}$ (using the pn spectra), respectively.

4.2 Phase-resolved spectroscopy

We performed a phase-resolved spectroscopy (PRS) for all the *XMM-Newton* observations. We generated 10 phase-resolved spectra for each observation using the ephemeris reported in §3. The choice of the number of intervals was made *a priori* in order to have enough statistics in each phase-resolved spectrum to detect, at a 3σ confidence level, a spectral line with an equivalent width $> 30 \text{ eV}$ (although none was detected). Note that given the phase-connection

Parameters	Blackbody + 2 Power-laws	
	2008-08-23	2008-08-29
N_H	0.91 ± 0.02	0.93 ± 0.03
kT (keV)	0.70 ± 0.02	0.69 ± 0.04
BB ₁ Radius (km)	1.4 ± 0.1	1.5 ± 0.3
BB ₁ flux	2.2 ± 0.1	2.7 ± 0.1
Γ_{soft}	2.92 ± 0.07	3.2 ± 0.1
PL _{soft} flux	8.3 ± 0.1	7.1 ± 0.2
Γ_{hard}	0.8 frozen	0.8 ± 0.2
PL _{hard} flux	3.5 ± 0.1	3.9 ± 0.2
Abs. flux	7.9 ± 0.1	6.8 ± 0.3
Unab. flux	14.3 ± 0.1	12.6 ± 0.3
χ^2_{ν} (d.o.f.)	1.17 (204)	1.18 (175)
F-test prob.	3.1×10^{-5}	4.1×10^{-8}

Table 3. Parameters of the spectral modelling of the phase-averaged spectra of the first two *XMM-Newton* observations of SGR 0501+4516 with a blackbody plus two power-laws. For the second observation we used the quasi-simultaneous *INTEGRAL* data (see also Fig. 8 and §2.2). N_H is in units of 10^{22} cm^{-2} , and the blackbody radius is calculated at infinity, assuming a distance of 5 kpc (uncertainties on the distance have not been included). The blackbody and power-law fluxes are calculated in the 0.5–100 keV band. Unless otherwise specified, fluxes are all unabsorbed and in units of $10^{-11} \text{ erg cm}^{-2} \text{ s}^{-1}$. Errors are at the 90% confidence level.

of all the 5 *XMM-Newton* observations (see §3), we can reliably follow each phase-resolved spectrum in time.

The absorbed BB plus PL model provides excellent fits for all ten phase-resolved spectra in all the observations, both when leaving N_H free and when fixing it to the most accurate value derived in the phase-averaged fitting of all five *XMM-Newton* observations (see Tab. 2). In Fig. 9 we have plotted the parameters derived from the PRS analysis and compared them to the pulse profile in each observation. All the observations showed significant spectral variability with phase, as well as a general softening in time. In particular, the blackbody temperature and normalization follow the pulse profile shape rather well, and remaining on average rather constant throughout the outburst, with a slightly decrease in the last *XMM-Newton* observation. On the other hand, the power-law parameters vary in phase and follow a more complex behaviour, with a double-peaked change of the photon index (see also Fig. 6, and §5 for further discussion).

5 DISCUSSION

In the last few years, thanks to the availability of wide field X-ray instruments, as *Swift*-BAT, several outbursts from known AXP and SGR have been observed, and monitored in great detail. The detection of an outburst from SGR 0501+4516 has a special significance since this is the first new SGR discovered over a decade. In this paper we presented a comprehensive study of the spectral and timing properties of the source in the X-rays during the entire

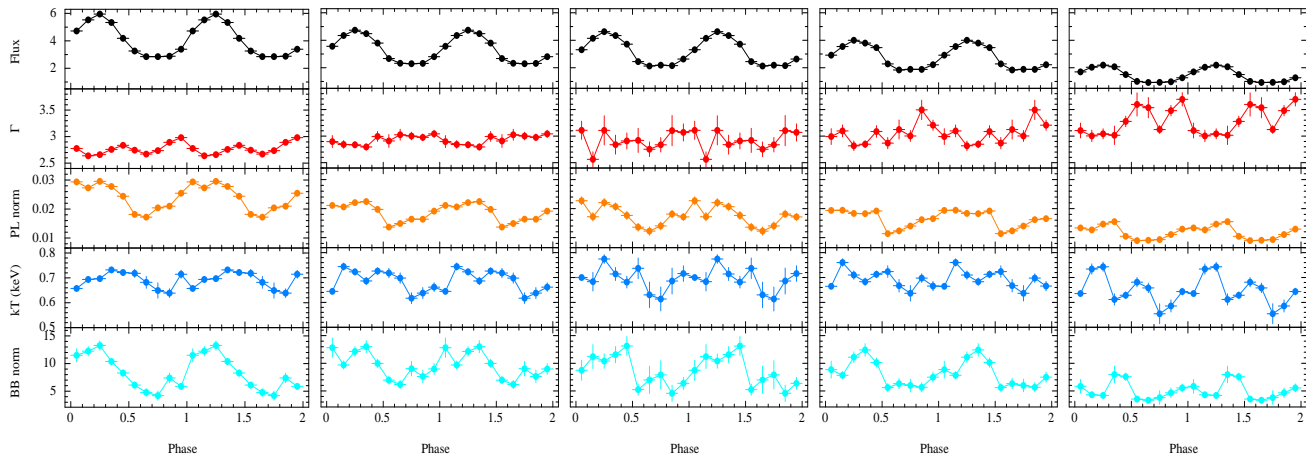


Figure 9. Phase-resolved spectroscopy: spectral parameters for each 0.1 phase-bin for all five observations (epoch increases from left to right). For each observation all phase-resolved spectra were fitted simultaneously with an absorbed blackbody plus a power-law, keeping the N_H fixed at the most accurate phase-averaged value ($N_H = (0.89 \pm 0.01) \times 10^{22} \text{cm}^{-2}$). Fluxes are absorbed, in the 0.5–10keV energy range and in units of $10^{-11} \text{erg s}^{-1} \text{cm}^{-2}$. Error bars are at the 90% confidence level.

evolution of the outburst, starting from ~ 1 day after the activation and up to ~ 160 days later. Our investigation is based on *XMM-Newton*, *Swift-XRT*, and *INTEGRAL* data and we also re-examined *ROSAT* archival data in which the quiescent emission of SGR 0501+4516 was detected.

5.1 The outburst evolution and timescale

Thanks to the *XMM-Newton* and *Swift-XRT* quasi-continuous monitoring (see §2.1 and §2.3), we could study in detail the flux decay of SGR 0501+4516 and give an estimate of its typical timescale. Fitting the flux evolution in the first 160 days after the onset of the bursting activity, we found that an exponential function of the form $\text{Flux}(t) = K_1 + K_2 \exp(-t/t_c)$ provides a good representation of the data ($\chi^2_\nu=1.2$); the best values of the parameters are $K_1 = (0.66 \pm 0.03) \times 10^{-11} \text{erg s}^{-1} \text{cm}^{-2}$, $K_2 = (3.52 \pm 0.02) \times 10^{-11} \text{erg s}^{-1} \text{cm}^{-2}$, and $t_c = 23.81 \pm 0.05$ days (see Fig. 3). A fit with a power-law was not found to be satisfactory ($\chi^2_\nu=12$). Comparing the outburst decay timescale of SGR 0501+4516 with other magnetars (see Fig. 11), there is a clear difference in timescales. In particular, the outburst decays of other magnetars are usually fitted by two components: an initial exponential or power-law component accounting for the very fast decrease in the first day or so (successfully observed only in a very few cases), followed by a much flatter power-law with an index of $\delta \sim 0.2 - 0.5$, where $\text{Flux}(t) = (t - t_0)^\delta$ (see Woods et al. 2004; Israel et al. 2007; Esposito et al. 2008). A pure exponential flux decay with a timescale of about 24 days is unusual and has been never observed before. However, we caveat that the source did not reach the quiescent level yet, hence a second component (e.g. a power-law) in the flux decay can still appear at later times. Further monitoring observations will allow in the future a complete modeling of the outburst decay until the quiescent source level.

From Tab. 2 and Fig. 6 it is apparent that, at least in the first ten days of the outburst, the flux of the blackbody component decayed more slowly than that of the power-law one, both in the phase-average and the phase-resolved spec-

tra. In particular, fitting the phase-average BB and PL fluxes of the first 4 *XMM-Newton* observations (see Tab. 2) with a linear function of the form $\text{Flux}(t) = A_1 + A_2 t$ we found a good fit for $A_1(PL) = 7.9(1) \times 10^{-11} \text{erg s}^{-1} \text{cm}^{-2}$ and $A_1(BB) = 2.2(1) \times 10^{-11} \text{erg s}^{-1} \text{cm}^{-2}$, and with $A_2(PL) = -0.29(1) \times 10^{-11} \text{erg s}^{-2} \text{cm}^{-2}$ and $A_2(BB) = -0.018(3) \times 10^{-11} \text{erg s}^{-2} \text{cm}^{-2}$. While the PL flux decreased by $\sim 25\%$ from the first to the second observation (and kept decreasing at a reduced rate in observations three and four), the BB flux stayed approximately constant during the first four observations. Both fluxes then substantially decreased in observation five (see also §4.2 and next section for the evolution of the phase-resolved spectra). The relative decays of the thermal and non-thermal components observed here are reminiscent of those of CXO J167410.2-455216 after its intense burst of 2006 September 21 (Muno et al. 2007; Israel et al. 2007). Even in that case, the PL component decayed more rapidly than the BB flux (Israel et al. 2007). The faster decay of the non-thermal emission from SGR 0501+4516 is also corroborated by the non-detection of the source in the second *INTEGRAL* pointing (see §4).

The transient character of the hard component we detected at the beginning of SGR 0501+4516's outburst implies that, whatever the mechanism is, thermal bremsstrahlung in the surface layers heated by returning currents, synchrotron emission from pairs created higher up (~ 100 km) in the magnetosphere (Thompson & Beloborodov 2005), or resonant up-scattering of seed photons on a population of highly relativistic electrons (Baring & Harding 2007), it has to be triggered by the source activity and quickly fade in a few days. All the previous scenarios are indeed compatible with the observed behaviour provided that a flow of highly relativistic particles is injected into the magnetosphere during the outburst. Note that this is the first time that a variable hard X-ray emission is detected for a magnetar during an outburst. Of course, our observations did not allow us to distinguish between a rapid spectral softening (as expected if the particles responsible for the emission becomes less and less energetic) and/or an overall fading of the hard component due to a decrease in its normalization

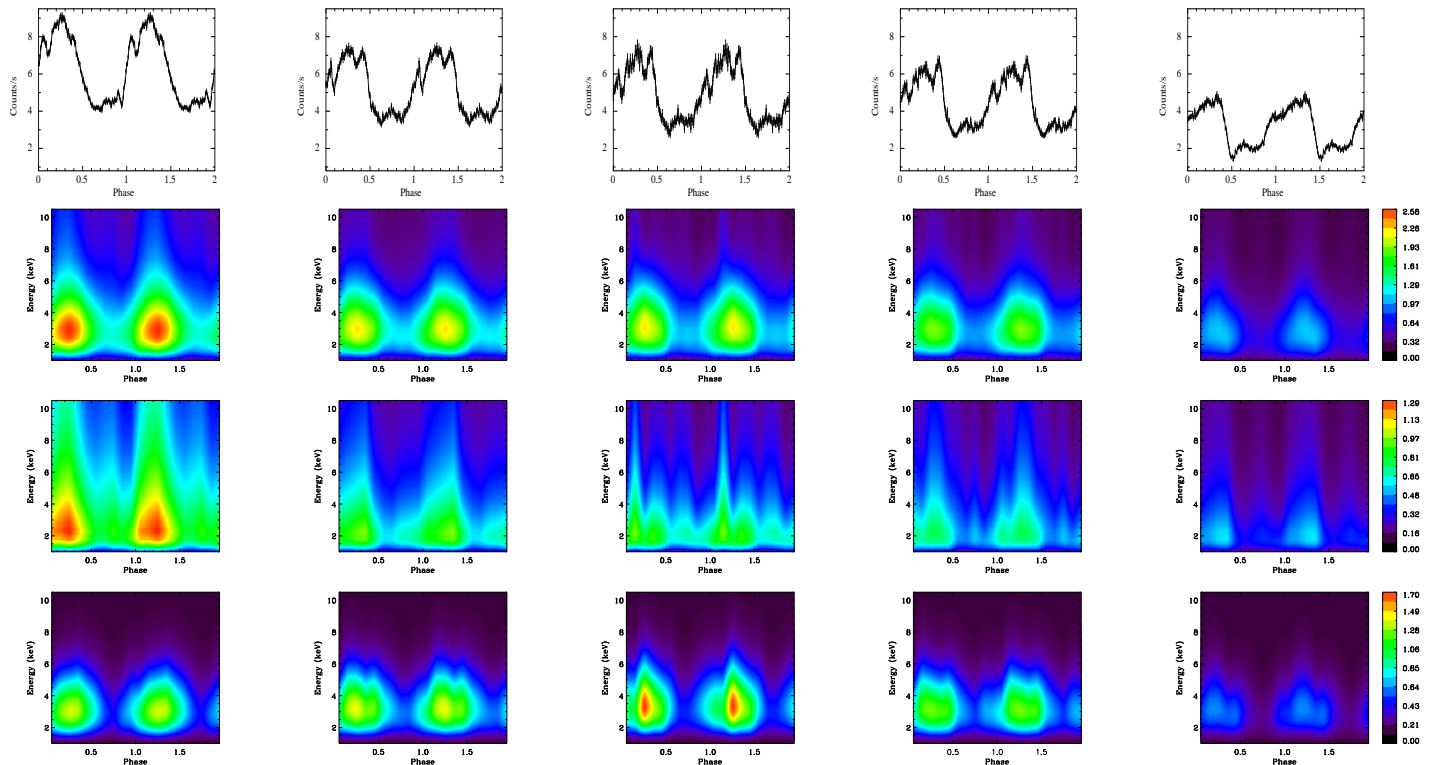


Figure 10. Dynamic Spectral Profiles (DSPs). Each column corresponds to one *XMM-Newton* observation (epoch increases from left to right: 2008 August 23, 29, 31, September 02 and 30). For each observation, the top panel is the 0.3–12 keV pulse profile, while the three bottom panels show in the phase/energy plane the contour plots for the total (second row), power-law (third row) and blackbody (bottom row) νF_ν flux. The colour scale is in units of $0.01 \text{ keV}/(\text{keV cm}^{-2} \text{ s}^{-1} \text{ keV}^{-1})$.

(as expected if the spatial region occupied/heated by such particles shrinks or if their local density decreases).

Several investigations have suggested that the observed magnetar spectra form in the magnetosphere, where thermal photons emitted from the neutron star’s surface undergo repeated resonant scatterings (Thompson, Lyutikov & Kulkarni 2002; Lyutikov & Gavril 2006; Fernandez & Thompson 2007; Rea et al. 2008; Nobili, Turolla & Zane 2008a). In this scenario, the spectral shape of the non-thermal component in the ~ 0.1 –10 keV band (and possibly also that at *INTEGRAL* energies; see Baring & Harding 2007, 2008; Nobili, Turolla & Zane 2008b) is governed by the amount of twist which is implanted in the magnetosphere as a consequence of large scale crustal motions (star-quakes). The twist must decay, due to resistive ohmic dissipation, in order to support its own currents (Beloborodov & Thompson 2007; Beloborodov 2009) and this, in turn, implies that the high-energy component of the spectrum has to fade. If either the initial twist is global or, as it seems more likely, it affects only a bundle of (closed) field lines (e.g. near a magnetic pole), the magnetosphere evolves in such a way as to confine the current-carrying ($\nabla \times \mathbf{B} \neq 0$) field lines closer to the magnetic axis (Beloborodov 2009). This necessarily quenches resonant up-scattering because the value of the cyclotron energy in most of the region occupied by the current-carrying field lines (which now extend to large radii) drops below ≈ 1 keV, the typical energy of thermal photons.

Thompson, Lyutikov & Kulkarni (2002) and Be-

loborodov & Thompson (2007) pointed out that the surface of a magnetar with a twisted magnetosphere is heated by the returning currents. If the twist decays, the luminosity and the area of the heated surface decrease in time. However, while the thermal component is expected to survive over the timescale necessary to dissipate the twist energy, the non-thermal component is more short-lived, since resonant scattering is no longer possible when the current-carrying bundle becomes too small. By comparing the theoretical expectations for a typical twist duration and luminosity, Beloborodov (2009) found an overall agreement with the observed properties of the transient AXP XTE J1810–197, provided that the twist was localized. In the case of SGR 0501+4516, the typical derived evolution time (~ 1 month) requires both a twist confined to a small volume (angular extent $\sin^2\theta \sim 0.1$) and a modest twist angle ($\psi \sim 0.1$). The distance of SGR 0501+4516 is not known yet, but it has recently been estimated to be ~ 1.5 kpc at the lowest (Aptekar et al. 2009), which implies a minimum source peak luminosity $L \gtrsim 2.5 \times 10^{34} \text{ erg s}^{-1}$. Under this case the values of the magnetospheric parameters derived above from the timescale of the outburst evolution are too small to explain the observed luminosity in terms of dissipation of the twist energy alone ($L_{\text{twist}} \sim 10^{33} \text{ erg s}^{-1}$), and the problem worsens if the source distance is larger (unless the emission has a beaming factor $\lesssim 0.1$). One possibility is that part of the energy has been released impulsively in the crust because of the dissipation of the toroidal field following the star-quake, as suggested to explain the decay

of SGR 1900+14 and SGR 1627–41 (Lyubarsky, Eichler & Thompson 2003; Kouveliotou et al. 2003). However, this scenario predicts a power-law luminosity decline, $L \sim (t - t_0)^\delta$, which is not observed in SGR 0501+4516. We note that the flux decay may follow different laws in the untwisting magnetosphere model of Beloborodov (2009), and the observed different decay timescales of the thermal and non-thermal components fits in the latter scenario.

5.2 Spectral variability with phase

To study the pulse profiles and the spectral changes in phase and time as a whole, we produced what we define hereafter as Dynamic Spectral Profiles (DSPs), which are shown in Fig. 10. Each column in Fig. 10 is for one of the 5 *XMM-Newton* observations (epoch increases from left to right). Each panel shows a contour plot of the νF_ν flux as a function of phase and energy, and has been derived from the 10 phase-resolved spectra extracted as explained above. The second row refers to the total flux, as derived from the BB+PL model, while the third and the last rows show, respectively, the flux of the PL and BB components. The plots illustrate well how the source spectrum changes as phase and time, and show a clear evolution of the phase-dependent spectrum during the outburst. At energies above ~ 5 keV the PL dominates the emission at all times. From the DSPs, and by comparing the DSPs with the pulse profiles (see Fig. 10 top panel and also Fig. 5), it is also evident that most of the sub-peaks of the pulse profiles are related to the PL component (this is particularly evident in the third and fourth *XMM-Newton* observations). On the other hand, the main component of the profiles is dominated by the BB component, which is always in phase with the main peak. Moreover, by looking at Fig. 10 it is again evident how the PL component decreases in intensity on a faster timescale than the BB component in all phases. Actually the BB component is not only rather constant over the first four observations (covering the first 10 days after the bursting activation), but in some phases shows a re-brightening (see Fig. 6, and the third panel in the last row of Fig. 10). This is likely due to some late heating of the surface, e.g. by returning currents.

The strong phase dependence of the non-thermal component may be explained by the fact that, in the twisted magnetosphere model, both the spatial distributions of the magnetospheric currents (which act as a “scattering medium”) and the surface emission induced by the returning currents (which acts as source of seed photons for the resonant scattering) are substantially anisotropic. Even under the simple assumption where the magnetosphere is dipolar and globally twisted, the heated part of the surface and the magnetospheric charges cover two different ranges of magnetic colatitude. If the twist angle varies during the outburst evolution, both distributions would move away or toward the poles but at different rates. Of course, the situation is more complicated if the magnetospheric twist affects a limited bundle of field lines, as observations seem to indicate in SGR 1806–20 (Woods et al. 2007) and in the transient AXP XTE J1810–197 (Perna & Gotthelf 2008; Bernardini et al. 2009). Recent spectral calculations have shown the resonant comptonization in locally twisted multipolar fields can give rise to a hard tail which is highly phase dependent (Pavan et al. 2009). The phase-resolved spectral evolution

of SGR 0501+4516 is very complicated, but a possible explanation for the variations of the PL component in terms of a magnetic field which is locally sheared, and the shear evolves in time, seems promising.

5.3 SGR 0501+4516: AXP or SGR?

For about 20 years after their discovery, SGRs and AXPs were thought to be two distinct manifestations of highly magnetic neutron stars: the first mainly discovered and characterized by their powerful bursting activity, and the second recognized as bright persistent soft X-ray emitters with spectra empirically modelled by a BB+PL, and with little or no bursting activity. Furthermore, the discovery of hard X-ray emission (up to about 200 keV; Kuiper et al. 2006; Götz et al. 2006) from a few members of both classes, added a further distinction, with AXPs having hard X-ray emission modelled by a second PL component (in addition to the BB+PL describing the soft X-ray emission) with $\Gamma_{\text{hard}} \sim 0.8 - 1$, while the SGR emission was the natural extrapolation at higher energies of the PL component modelling their soft X-ray emission ($\Gamma_{\text{hard}} \sim 1.5 - 2.0$). Over the past 6 years, the discovery of X-ray bursts from AXPs (Kaspi et al. 2003; Woods et al. 2004), and of BB components in the persistent spectrum of SGRs (Mereghetti et al. 2005, 2006a), initiated a revision of this distinction between these two classes.

In this context SGR 0501+4516 and 1E 1547.0-5408 can be considered the Rosetta stone for a final unification of SGRs, AXPs and the so called “transient AXPs (TAXPs)”, into a single class of “magnetars candidates”. In fact the properties of this new SGR, as well as the characteristics of the 2009 January 22 outburst of the AXP 1E 1547.0-5408 (Gelfand & Gaensler 2007; Halpern et al. 2008; Mereghetti et al. 2009; Israel et al. 2009 in prep), argue for a revision of our definition of SGRs and AXPs. In particular, SGR 0501+4516’s 0.5-10 keV spectrum during outburst, is extremely soft ($\Gamma \sim 2.8-3.0$) compared to other SGRs ($\Gamma \sim 1.5-2.0$). Such a soft spectrum has been observed in the persistent emission of SGRs only during the “quiescent” (burst-quiet) phases of SGR 1627–41 and SGR 0526–66 (Kouveliotou et al. 2003; Kulkarni et al. 2003; Mereghetti et al. 2006b). Furthermore, the spectrum of the quiescent X-ray counterpart of SGR 0501+4516 (see §2.4 and §4) is far too soft for an SGR, while resemble the pre-outburst spectrum of the transient AXP XTE J1810–197 (Gotthelf et al. 2004).

The name SGR 0501+4516 came from the strong bursting activity (see e.g. Enoto et al. 2009; Aptekar et al. 2009) which led to its discovery. However, bursts as bright and numerous as those observed from this source and other SGRs, have recently been observed from the AXP 1E 1547.0-5408 in January 2009 (Gronwall et al. 2009; Savchenko et al. 2009; von Kienlin & Connaughton 2009), which emitted bursts as powerful as a typical SGR intermediate flares (Mereghetti et al. 2009).

Another piece of evidence for the AXP-like behaviour of SGR 0501+4516, and the SGR-like behaviour of 1E 1547.0-5408 is the photon index of the variable hard X-ray component. As shown in §4 the photon index we measure from the *INTEGRAL* spectrum is $\Gamma \sim 0.8$, which is close to the one reported for AXPs, while the variable hard X-ray emission during the January 2009 outburst of 1E 1547.0-5408 has a

photon index of $\Gamma \sim 1.4 - 1.6$ (den Hartog et al. 2009), typical of SGRs.

6 SUMMARY

Thanks to the unprecedented prompt observational campaigns of *XMM-Newton*, *INTEGRAL*, and *Swift*, we were able to study in great detail the evolution of the first recorded outburst from the first new SGR discovered in a decade, SGR 0501+4516. Furthermore, we could compare its outburst properties with its quiescent emission as seen by *ROSAT*. We found the following.

- Phase-connected timing analysis of the entire X-ray outburst of SGR 0501+4516, strongly argue that this source is a magnetar candidate with a magnetic field of $B \sim 2 \times 10^{14}$ Gauss. Furthermore, we identified a negative second period derivative of $\dot{P} = -1.6(4) \times 10^{-19} \text{ s s}^{-2}$ which implies that the spin-down rate is decreasing with time, possibly in its way to recovering to its secular pre-outburst spin-down.

- A variable hard X-ray component was detected at the beginning of the outburst (see Fig. 8), and became undetectable by *INTEGRAL* some time within 10 days after the on-set of the bursting activity. This represent the first detection of a variable hard X-ray component in a magnetar over such a short timescale.

- The phase-connection of all the observations allowed us to study the evolution in time of the phase-resolved spectra. We found that on top of a phase-averaged spectral softening during the outburst decay, with the BB component decaying on a slower timescale than the PL component (see Fig. 6), the spectral evolution also changes from phase to phase. The main peak of the pulse profile is dominated by the thermal component, while many other sub-peaks are present in the profiles, which are dominated instead by the non-thermal component (see Fig. 10).

- No transient optical/ultraviolet source was detected by the Optical Monitor on board of *XMM-Newton* (see §2.1.2). Note that the optical counterpart to this source (Tanvir et al. 2008; Fatkhullin et al. 2008) is too faint to be observable by the OM, but we could constrain that no counterpart to the X-ray bursts have been observed with $m_{UVW1} > 22.05$.

- From a comparison with other outbursts recently detected from SGRs and AXPs (see Fig. 11), we show that contrary to other sources, in the first 160 days of its outburst, SGR 0501+4516 shows a clear exponential decay on a rather slow timescale of about 24 days (see Fig. 3).

- The discovery of SGR 0501+4516, and its AXP-like characteristics, represents another piece of evidence in the unification of the magnetar candidate class, weakening further the differences between AXPs, TAXPs, and SGRs.

ACKNOWLEDGEMENTS

We wish to thank Norbert Schartel for promptly approving our ToO request for the first *XMM-Newton* observation, the *XMM-Newton* team for the crucial help during the scheduling process of this monitoring program, and the *INTEGRAL* mission operations team at ISOC and ESOC for

their support during the ToO observations. We also thank Neil Gehrels, the *Swift* duty scientists and science planners for making the *Swift* observations possible. This paper is based on observations obtained with *XMM-Newton* and *INTEGRAL*, which are both ESA science missions with instruments and contributions directly funded by ESA Member States and the USA (through NASA), and on observations with the NASA/UK/ASI *Swift* mission. NR is supported by an NWO Veni Fellowship and thanks T. Enoto and K. Makishima for useful discussions on this source. PE thanks the Osio Sotto city council for support with a G. Petrocchi Fellowship, SZ acknowledges STFC for support through an Advanced Fellowship, KH is grateful to the U.S. *INTEGRAL* Guest Investigator program for support under NASA Grant NNX08AC89G, and PU has been supported by the Italian Space Agency through the *INTEGRAL* grant I/008/07/0.

REFERENCES

- Anders, E., & Grevesse, N. 1989, 53, 197
- Aptekar, R.L., Cline, T.L., Frederiks, D.D., Golenetskii, S.V., Mazets, E.P., Pal'shin, V.D., 2009, ApJ, submitted (arXiv:0902.3391)
- Balucinska-Church, M. & McCammon, D. 1998, ApJ, 496, 1044
- Baring, M.G. & Harding, A.K., 2007, Ap&SS, 308, 109
- Baring, M.G. & Harding, A.K., 2008, AIP Conference Proceedings, 968, 93
- Barthelmy, S. D., et al. 2005, Space Science Reviews, 120, 143
- Barthelmy, S. D., et al. 2008, The Astronomer's Telegram, 1676
- Beloborodov A. M., Thompson C. 2007, ApJ, 657, 967
- Beloborodov A. M., 2009, ApJ, in press [arXiv:0812.4873]
- Bernardini, F., et al. 2009, A&A in press., arXiv:0901.2241
- Burrows, D. N., et al. 2005, Space Science Reviews, 120, 165
- Chatterjee, P., Hernquist, L., & Narayan, R. 2000, ApJ, 534, 373
- Dall'Osso, S., Israel, G. L., Stella, L., Possenti, A., & Peruzzi, E. 2003, ApJ, 599, 485
- den Hartog, P. R., Kuiper, L., & Hermsen, W. 2009, The Astronomer's Telegram, 1922
- den Herder, J. W., et al. 2001, ApJ, 365, L7
- Dib, R., Kaspi, V. M., & Gavriil, F. P. 2008, ApJ, 673, 1044
- Duncan, R., Thompson, C. 1992, ApJ, 392, L9
- Eichler, D., et al., 2006, arXiv:astro-ph/06111747
- Enoto, T., et al. 2009, ApJ, 693, L122
- Esposito, P., et al., 2008, MNRAS, 390, L34
- Fatkhullin, T., et al. 2008, GRB Coordinates Network, 8160
- Fernandez R., & Thompson C., 2007, ApJ, 660, 615
- Feroci, M., et al. 2008, The Astronomer's Telegram, 1705
- Gelfand, J. D., & Gaensler, B. M. 2007, ApJ, 667, 1111
- Gelfand, J. D., Taylor, G., Kouveliotou, C., Gaensler, B., & van der Horst, A. J. 2008, GRB Coordinates Network, 8168
- Gehrels, N., & Swift Team 2004, Gamma-Ray Bursts: 30 Years of Discovery, 727, 637
- Gogus, E., Woods, P., & Kouveliotou, C. 2008, The Astronomer's Telegram, 1677

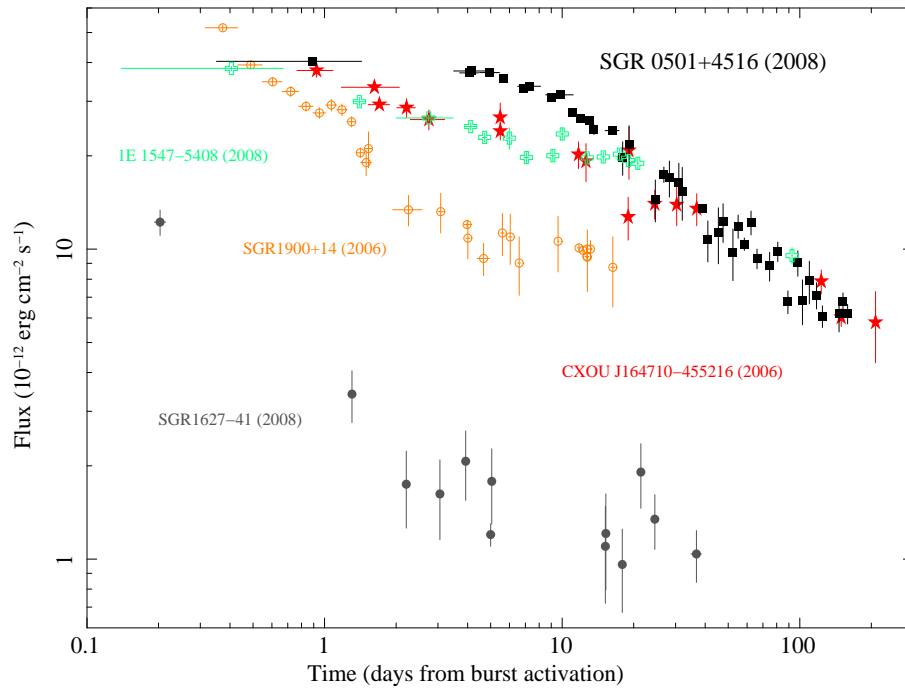


Figure 11. Flux evolution of the recent outbursts of a few magnetars (all observed with imaging instruments) compared with SGR 0501+4516. Fluxes are the observed ones in the 1-10keV energy range, and the reported times are calculated in days from the detection of the first burst in each source. In particular we show CXOU J164710.2-455216 as red stars (Israel et al. 2007), SGR 1627-41 as grey circles (Esposito et al. 2008), SGR 1900+14 as orange empty circles (Israel et al. 2008), 1E 1547.0-5408 as green empty crosses (Israel et al. in prep), and SGR 0501+4516 as black squares (this work).

Gotthelf, E. V., Halpern, J. P., Buxton, M., & Bailyn, C. 2004, *ApJ*, 605, 368
 Götz, D., et al., 2006, *A&A*, 449, L31
 Gronwall, C., et al. 2009, GRB Coordinates Network, 8833
 Halpern, J.P., Gotthelf, E.V., Reynolds, J., Ransom, S.M., Camilo, F. 2008, *ApJ*, 676, 1178
 Hessels, J., Rea, N., Ransom, S., & Stappers, B. 2008, GRB Coordinates Network, 8134
 Holland, S. T., et al. 2008, GRB Coordinates Network, 8112
 Hurley, K., et al., 1999, *Nature*, 397, 41
 Hurley, K., et al., 2005, *Nature*, 434, 1098
 Israel, G.L., et al., 2007, *ApJ*, 664, 448
 Israel, G. L., et al. 2008a, *The Astronomer’s Telegram*, 1837
 Jansen, F., et al. 2001, *ApJ*, 365, L1
 Kaspi, V. M., Gavriil, F. P., Woods, P. M., Jensen, J. B., Roberts, M. S. E., & Chakrabarty, D. 2003, *ApJ*, 588, L93
 Kaspi, V., 2007, *Ap&SS*, 308, 1
 Kouveliotou, C. et al. 2003, *ApJ*, 596, L79
 Kuiper, L., Hermsen, W., & Mendez, M., 2004, *ApJ*, 613, 1173
 Kuiper, L., et al., 2006, *ApJ*, 645, 556
 Kulkarni, S. R., Kaplan, D. L., Marshall, H. L., Frail, D. A., Murakami, T., & Yonetoku, D. 2003, *ApJ*, 585, 948
 Kulkarni, S. R., & Frail, D. A. 2008, GRB Coordinates Network, 8130
 Lebrun, F., Leray, J.P., Lavocat, P., et al. 2003, *A&A*, 411, L141
 Lyubarsky, Y., Eichler, D. & Thompson, C. 2003, *ApJ*, 580, L69
 Lyutikov, M. 2003, *MNRAS*, 346, 540
 Lyutikov M., & Gavriil F.P. 2006, *MNRAS*, 368, 690

Mason, K. O., et al. 2001, *A&A*, 365, L36
 Mazets, E.P., et al., 1979, *Nature*, 282, 587
 Mereghetti, S., et al., 2005, *A&A*, 433, L9
 Mereghetti, S., et al. 2006a, *ApJ*, 450, 759
 Mereghetti, S., et al. 2006b, *ApJ*, 653, 1423
 Mereghetti, S., 2008, *A&A Review*, 15, 225
 Mereghetti, S., et al. 2009, *ApJ* submitted
 Monet, D. G., et al. 2003, *AJ*, 125, 984
 Munro, M. P., Gaensler, B. M., Clark, J. S., de Grijs, R., Pooley, D., Stevens, I. R., & Portegies Zwart, S. F. 2007, *MNRAS*, 378, L44
 Nobili L., Turolla R., & Zane S. 2008a, *MNRAS*, 386, 1527
 Nobili L., Turolla R., & Zane S. 2008b, *MNRAS*, 389, 989
 Ouyed, R., Leahy, D., & Niebergal, B. 2007a, *A&A*, 473, 357
 Ouyed, R., Leahy, D., & Niebergal, B. 2007b, *A&A*, 475, 73
 Palmer, D.M., et al., 2005, *Nature*, 434, 1107
 Pavan, L., et al., 2009, *MNRAS* in press, arXiv:0902.0720
 Perna, R., Hernquist, L., & Narayan, R. 2000, *ApJ*, 541, 344
 Rea, N., Zane, S., Turolla, R., Lyutikov, M., Götz, D. 2008, *ApJ*, 686, 1245
 Rea, N., Rol, E., Curran, P. A., Skillen, I., Russell, D. M., & Israel, G. L. 2008b, GRB Coordinates Network, 8159
 Rol, E., Tanvir, N., Rea, N., Wiersema, K., Skillen, I., & Curran, P. A. 2008, GRB Coordinates Network, 8164
 Roming, P. W. A., et al. 2005, *Space Science Reviews*, 120, 95
 Savchenko, V., et al. 2009, GRB Coordinates Network 8837
 Snowden, S. L., & Schmitt, J. H. M. M. 1990, *ApJS*, 171,

207

- Strüder, L., et al. 2001, ApJ, 365, L18
Tanvir, N. R., & Varricatt, W. 2008, GRB Coordinates Network, 8126
Thompson C., & Beloborodov, A.M., 2005, ApJ, 634, 565
Thompson C., & Duncan, R.C., 1993, ApJ, 408, 194
Thompson, C., & Duncan, R. C. 1995, MNRAS, 275, 255
Thompson C., Lyutikov M., & Kulkarni S.R., 2002, ApJ, 274, 332
Turner, M. J. L., et al. 2001, ApJ, 365, L27
Ubertini, P., Lebrun, F., Di Cocco, G., et al. 2003, A&A, 411, L131
Voges, W., et al. 1992, Environment Observation and Climate Modelling Through International Space Projects, 223
von Kienlin, A. & Connaughton, V. 2009, GRB Coordinates Network 8838
Winkler, C., Courvoisier, T.J.-L., Di Cocco G., et al. 2003 A&A, 411, L1
Woods P.M. et al. 2004, ApJ, 605, 378
Woods P.M. et al. 2007, ApJ, 654, 470
Woods, P., Gogus, E., & Kouveliotou, C. 2008, The Astronomer's Telegram, 1824